Elucidating Salt Conversion Mechanisms of Lithiated Transition Metal Oxide for Lithium-ion Batteries Recycling

Lydia Hamitouche, Clara Robert, Anne-Laure Rollet, Valérie Briois, Mohamed Selmane, Ana Gabriela Porras Gutierrez, Sandrine Leclerc, Denise Krulic, Nicolas Fatouros, Juliette Sirieix-Plénet, et al.

Elucidating Salt Conversion Mechanisms of Lithiated Transition Metal Oxide for Lithium-ion Batteries Recycling

Lydia Hamitouche[1,2], Clara Robert[2,3], Anne-Laure Rollet[1,2], Valérie Briois[4], Mohamed Selmane[5], Ana Gabriela Porras Gutierrez[1,2], Sandrine Leclerc[1,2], Denise Krulic[1,2], Nicolas Fatouros[1,2], Juliette Sirieix-Plénet[1,2], Laurent Michot[1,2], Marie-Liesse Doublet[2,3], and Damien Dambournet*[1,2].

[1] Sorbonne Université, CNRS, Physico-chimie des électrolytes et nano-systèmes interfaciaux, PHENIX, F-75005 Paris, France

[2] Réseau sur le Stockage Electrochimique de l'Energie (RS2E), FR CNRS 3459, 80039 Amiens cedex, France

[3] Univ Montpellier, Inst Charles Gerhardt Montpellier ICGM, CNRS, ENSCM, F-34293 Montpellier, France

[4] Synchrotron SOLEIL L'orme des Merisiers, BP48, 91192, Gif-sur-Yvette Cedex, France

[5] Sorbonne Université, Fédération de Chimie et Matériaux de Paris Centre (FCMat), Paris, Cedex 05, 75252, France

ABSTRACT: Exploring new methods for recycling spent Li-ion batteries is mandatory for facing the on-going growing demand for strategic elements. Here, we propose a method to chemically convert lithiated transition metal oxides into readily water-soluble sulfate products, preventing the use of highly acidic media typically used in hydrometallurgy. The process englobes a temperature-driven solid-state reaction between the electrode material and the low-cost potassium hydrogenosulfate molten salt yielding langbeinite $K_2M_2(SO_4)_3$ and potassium/lithium sulfates. The salt conversion of the prototype material $LiCoO_2$ was elucidated highlighting a complex mechanism. Prior to the melting of the salt, we pointed out an ionic exchange occurring between Li ions and protons from $LiCoO_2$ and $KHSO_4$ reactants. The accumulation of protons within the layered structure is followed by thermal dehydration, leaving under-coordinated Co ions. Concomitantly, the melting of the salt provides reactive species such as HSO_4^-, leading to the progressive sulfation of Co ions as revealed by the formation of an intermediate reduced hydroxyl-sulfate phase followed by the final stabilization of $K_2Co_2(SO_4)_3$. Most remarkably, we highlight the compositional versatility of the langbeinite $K_2M_2(SO_4)_3$ by extending this approach to more complex cathode chemistry with nickel and manganese (NMC, NCA), which opens novel insights into versatile recycling methods featuring lower atom consumption.

INTRODUCTION

The energy transition will be accompanied by a boom in the use of mineral resources, as the demand for some metals could be multiplied by 10 by 2050[1]. In that context, lithium-ion batteries (LIB) mostly relies on positive electrode materials consisting of lithiated transition metal oxide (LCO: $LiCoO_2$, NCA: $LiNi_xCo_yAl_zO_2$, NMC: $LiNi_xMn_yCo_zO_2$, LMO: $LiMn_2O_4$) containing elements (lithium, cobalt, nickel) whose resources are limited and whose supply could become critical in view of the increasing demand of energy storage devices[2,3]. To overcome this criticality and the energy costs and environmental hazards associated with the extraction of these elements, large scale recycling is mandatory. The industrial recycling processes of positive electrode materials comprise pyrometallurgy and hydrometallurgy while direct recycling is still at the lab stage of development[4–7].

In hydrometallurgical processes, leaching enables the solubilization of positive electrode materials required to recover the target elements. Due to the low solubility of transition metals oxides in high oxidation states[7], acidic leaching in the presence of a reducing agent is commonly used. One can differentiate the use of inorganic (sulfuric, nitric, hydrochloric) organic (oxalic, citric, ascorbic, etc) acids and more recently deep eutectic solvents[8] as a possible alternative. An exhaustive literature overview of the acid leaching conditions provided by Zhang et *al*[9] highlighted the typical operative conditions as: concentrated acid medium (2-4 $mol.L^{-1}$), use of H_2O_2 as reducing agent for Co^{3+}, operating temperature from 25 to 90 °C, duration time from ten minutes to hours and mass of active material concentration from 2 to 200 $g.L^{-1}$.

To limit the extensive amount of chemicals used in hydrometallurgy, an alternative approach has emerged consisting in solid-state reactions to convert oxide-based materials into salts that are readily soluble in aqueous media. This approach hereafter denoted salt conversion, has already been demonstrated for different salts including sulfates[10]. In this latter case, different salts have been used such as $NaHSO_4.H_2O$[11,12] and $(NH_4)_2SO_4$[13,14]. These salts feature low melting points which favor their reactivity with layered oxide materials and parameters such as the temperature and the molar ratio between the salt and the oxide material, have been established to strongly impact the nature of the stabilized products. Most strikingly, the solid-state conversion resulted in the stabilization of transi-

tion metal reduced phases, *i.e.*, for instance $Na_6Co(SO_4)_4$, $Na_2Co(SO_4)_2$.

The salt conversion approach appears as a new recycling process enabling an atom economy, provided that a better understanding about the reactivity of layered oxide materials with these particular molten salt media is demonstrated. In this paper, we focus on the fundamental understanding of the reactivity of layered compounds with these media. Potassium hydrogenosultate ($KHSO_4$) was selected as the reactant as it has a melting point of about 200°C[15], at a pressure of 1 bar and because the K-Co-SO_4 ternary system has only one composition, $K_2M_2(SO_4)_3$, contrarily to the ternary system Na-Co-SO_4, featuring up to three compositions[16–18]. The langbeinite-type structure can accommodate different cations such as M = Mg^{2+}, Ca^{2+}, Mn^{2+}, Fe^{2+}, Co^{2+}, Ni^{2+}, Zn^{2+} and Cd^{2+},[19–25] and consists of corner-shared MO_6 polyhedra with SO_4 tetrahedra and potassium atoms located in large cavities **(Figure 1a)**. Speer et *al*,[19] discussed the structural dependence on the nature of M and found that it is only related to the degree of distortion of the MO_6 polyhedra. This is confirmed by the linear correlation between the cubic unit cell parameter and the M^{II} ionic radius **(Figure 1b)**. Hence, we anticipate that the transition metals of interest (Ni, Co, Mn) could be stabilized in this structure, irrespective of the chemical composition of the electrode materials.

In this study, we established the conditions to convert layered lithiated transition metal compounds into sulfates-based products targeting the stabilization of the metal into the langbeinite structure $K_2M_2(SO_4)_3$. We dig into the reaction mechanism occurring with the prototypic compound $LiCoO_2$ using a range of *in situ* methods and DFT-calculations highlighting complex reaction pathways. We further show that the salt conversion method can be extended to polycationic electrode chemistry (NMC, NCA) opening perspectives into a versatile recycling process for Li-ion batteries while providing novel insights into the reactivity of positive electrode materials.

METHODS

Solid-state reaction between electrode materials and potassium hydrogenosulfate. Electrode materials LCO, NCA and NMC were purchased from MTI Corporation. The purity was checked by XRD. The nominal composition of NCA and NMC was confirmed by Energy-dispersive X-ray spectroscopy (EDX). $KHSO_4$ was purchased from Sigma-Aldrich and the phase purity was confirmed by XRD. The molar ratio between electrode materials and hydrogenosulfates was set to 1:3 to ensure the completion of the reaction. The powders were thoroughly mixed in an agate mortar. The homogenous mixture was placed in an agate crucible. The heat treatment was performed under air using a heating ramp of 3.5 °C/ min up to 400 °C. The reaction was left to proceed for 4 hours and then cooled down to room temperature. The recovered powder was crushed and milled in an agate mortar and analyzed by X-ray diffraction.

X-ray powder diffraction analysis. XRD was carried out using a Bruker D8 ADVANCE X-ray diffractometer equipped with a Cu Kα radiation source (λ_1 = 1.54056 Å, λ_2 = 1.54439 Å) and 1D LynxEye detector. The sample powder was placed in a standard specimen holder in PMMA. The acquisition was carried out from 10° to 120° with 0.02° step size and 170 s step time. Powder patterns were refined using the Rietveld method as implemented in the FullProf program[26].

Thermal analyses. Thermogravimetric analysis (TGA) coupled with mass spectroscopy was performed using Netzsch STA 449F3. The experiment was carried out on Pt-Rh+Al_2O_3 under a flow of 40-20 ml min^{1} of argon. The temperature was increased to 500 °C with heating rate of 5 °C /min. Mass spectroscopy analysis was conducted by sweeping the scan energy (eV) for m/z from 1 to 10 at a rate of 20 ms per m/z and a resting time of 1 s.

The connection between TGA and MS was done by a stainless-steel capillary heated at 230°C.

Differential Scanning Calorimetry. DSC measurements were performed on a NETZSCH DSC 204F1 differential scanning calorimeter. The sample was placed on Al pan with pierced lid, and heated to 400°C at 5°C min^{-1}, under flow of 50 ml min^{-1} of argon.

Variable-temperature X-ray diffraction analysis. The variable-temperature XRD analysis was performed in reflection mode using a Bruker D8 DISCOVER X-ray diffractometer equipped with a Cu Kα radiation source (λ_1 = 1.54056 Å, λ_2 = 1.54439 Å) and 1D LynxEye detector. The [$LiCoO_2$: 3$KHSO_4$] mixture was placed in a ceramic sample holder. Throughout the analysis, the mixture was heated from 30°C to 220°C, with a

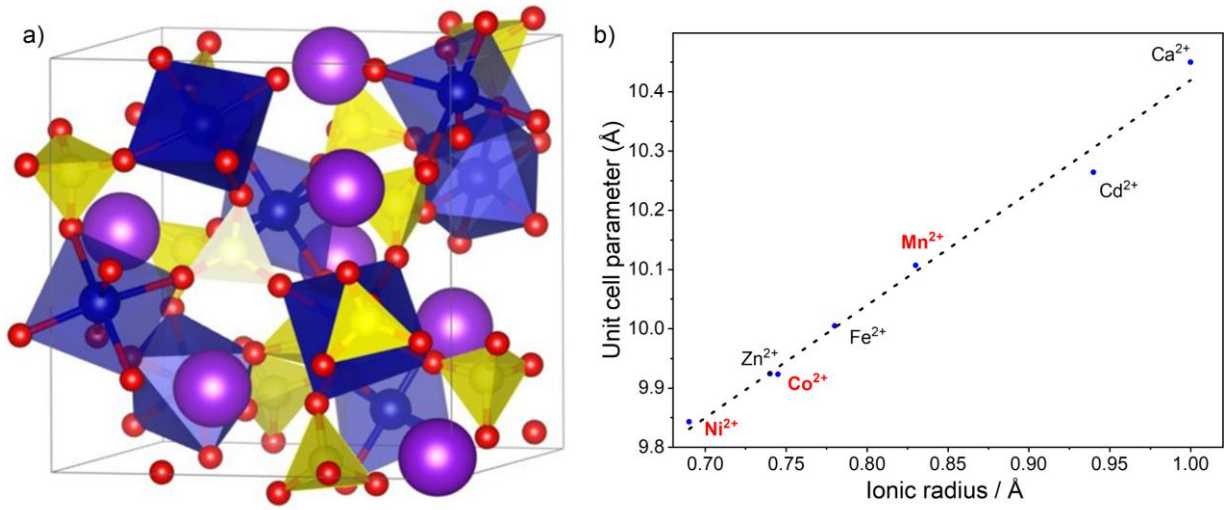

Figure 1. a) Cubic structure of $K_2M_2(SO_4)_3$ where red and purple spheres refer to oxygen and potassium atoms, respectively. Blue octahedra and yellow tetrahedra refer to MO_6 and SO_4, respectively. b) Cubic unit cell parameter versus ionic radius of M^{II}.

controlled heating rate of 5 °C/min.The acquisition was performed from 12° to 37° with 0.01° step size and 38.4 s step time and XRD patterns were collected each 5 °C.

In situ X-ray Absorption spectroscopy. A temperature-controlled *in situ* X-ray absorption spectroscopy experiment was performed at the K-edge of cobalt *i.e.*, 7709 eV, at the ROCK Quick-EXAFS beamline of the synchrotron Soleil (France). $LiCoO_2$ and $KHSO_4$ were mixed and pressed into a pellet, which was placed in a home-made cell[27] designed for *in situ* experiments and heated using a heating rate of 5°C/min from room temperature to 400 °C. XAS spectra were acquired in transmission mode with three ionization chambers: one before the sample, to measure the incident intensity, a second after the sample for measuring the transmitted intensity and a third one located after a Co metallic foil used as internal reference for further energy calibration. The energy was calibrated at 7709 eV at the maximum of the first derivative measured for the Co metallic foil. Measurement were performed over the range 7510-8300 eV using a 1.5° oscillation amplitude of the Si(111) channel-cut quick-EXAFS monochromator at 2Hz of frequency oscillation allowing the measurement of one spectrum in 250 ms. 800 spectra were collected during the heating ramp.

DFT-calculations. Spin-polarized density functional theory (DFT) calculations as implemented in VASP (Vienna ab initio simulation package)[28,29] were performed, using the projected augmented wave method (PAW).[30] The generalized gradient approximation of Perdew−Burke−Ernzerhof (PBE)[31] in conjunction with the rotationally invariant Dudarev method (DFT+U)[32] with U_{eff} = 3eV for Co. Different model structures were used to check the impact of Li/Li_{vac} or Li/H distributions in the alkali layers. In order to compare the energy of the Li-defective and Li/H-substituted $LiCoO_2$, their relative energy was computed following:

$$\Delta E = E(Li_{1-x}H_xCoO_2) - E(Li_{1-x}CoO_2 + \frac{x}{2}E(H_2)$$

The reference energy of H_2 was computed in a periodic cell of 20 $Å^3$ using large energy cutoff and k-point grid.

Metals recovery. The sulfate-based product was dissolved in milli-Q water at ambient temperature with a concentration of 0.24 mol/L of Co and Li ions. First, an aqueous solution of $K_2C_2O_4$ (0.29 mol/L) was added to the solution with a molar ratio of 1.2 between the oxalate ions ($C_2O_4^{2-}$) and cobalt ions (Co^{2+}), leading to the formation of a heterogenous solution with a pink precipitate. After 1 hour of agitation at 50 °C, the solid was filtered, dried and analyzed by XRD. To determine the yield of the reaction, Co ions was titrated by complexometry[33]. Sulfates were removed by the addition of an aqueous solution of $BaCl_2$ with a fixed barium/sulfate molar ratio equals to one. After stirring for one hour at room temperature, $BaSO_4$ was separated by centrifugation. Finally, lithium was recovered as a phosphate salt using the following protocol. The pH was adjusted to 12 using ammonia. Then an aqueous solution of $(NH_4)_3PO_4$, corresponding to a molar ratio of phosphate/lithium of 3.6, was slowly added to the solution. After stirring for one hour at 50 °C, the precipitate was recovered by centrifugation, washed with distilled water and analyzed by XRD after drying.

RESULTS AND DISCUSSION

Salt conversion of $LiCoO_2$ using $KHSO_4$

To probe the reactivity of $LiCoO_2$ with $KHSO_4$ seeking the complete conversion of oxide to sulfates (sulfation), solid-state reactions were performed under air with varying contents of the salt noted as $n \cdot KHSO_4$. The temperature was set to 400 °C, beyond which an onset of the sulfate decomposition was observed. The evolution of the most intense Bragg (003) reflection of $LiCoO_2$ was monitored as a function of *n*, as shown in **Figure 2a**. For n =1, the intensity of the peak strongly decreases. By increasing the $KHSO_4$ content (patterns [1: 1.5] and [1: 2]), the intensity of the (003) line further decreases. Still, a small peak assigned to Co_3O_4, *i.e.*, $Co^{II}Co^{III}{}_2O_4$ space group (SG): F d -3 m, was detected, indicating incomplete sulfation. Consequently, the $LiCoO_2$ /$KHSO_4$ ratio was set to 3 (pattern [1: 3]) yielding the complete disappearance of oxide compounds. The corresponding XRD pattern was indexed with sulfates products $K_2Co_2(SO_4)_3$, $KLiSO_4$ and K_2SO_4 demonstrating that the conversion is quantitative.

To establish the sulfation equation of $LiCoO_2$ with 3 $KHSO_4$, quantitative-phase analysis was deduced from Rietveld refinement of the XRD pattern and from thermogravimetric analysis coupled with mass spectrometry (TGA-MS).

The Rietveld refinement was performed using the Thompson-Cox-Hastings pseudo-Voigt function with the three-phases mentioned above, namely $K_2Co_2(SO_4)_3$, $KLiSO_4$ and K_2SO_4. The Rietveld refinement shown in **Figure 2b** reveals a good agreement between the observed XRD pattern (Yobs) and the theoretical pattern (Ycalc) with satisfactory reliability parameters. All peaks were indexed confirming a complete conversion of $LiCoO_2$ into sulfate-based products. The structural parameters obtained from the Rietveld analysis were gathered in **Table S1** and are in good agreement with literature data[34–36].

The thermogravimetric experiment coupled with mass spectrometry (TGA-MS) was performed on a [$LiCoO_2$: 3$KHSO_4$] mixture heated from RT to 500°C with a heating rate of 5°C/min. The obtained TGA curve **(Figure 3)** shows a continuous weight loss from 190°C to 400°C. The quasi-multiple ion detection (QMDI) curves indicate the release of H_2O^+ (m/z =18) and O_2^+ (m/z=32). The departure of water molecules spreads over a large range of temperature from 190 to 400°C, while the departure of oxygen is marked by a fine and intense peak at 350°C. Comparatively, the thermal behavior of $KHSO_4$ **(Figure S1)** showed only the departure of water suggesting that the release of molecular oxygen arises from the oxide lattice of $LiCoO_2$. Beyond 400 °C, the release of SO_2^+ (m/z = 64) was detected. Such a departure can induce a deficit of sulfate leading to an incomplete sulfation of $LiCoO_2$. Thus, the control of the temperature is mandatory to fully convert $LiCoO_2$ into sulfates-based products.

According to the quantitative-phase analysis determined by Rietveld refinement and the departure of H_2O and O_2, the

overall sulfation reaction can be established according to **eq.1.** The calculated weight percentages of the three phases are in good agreement with those determined experimentally by Rietveld analysis **(Table S1).**

$$LiCoO_2 + 3\,KHSO_4 \rightarrow \frac{1}{2}\,K_2Co_2(SO_4)_3 + KLiSO_4 + \frac{1}{2}\,K_2SO_4 + \frac{1}{4}O_{2(g)} + \frac{3}{2}\,H_2O_{(g)}$$ **(eq.1)**

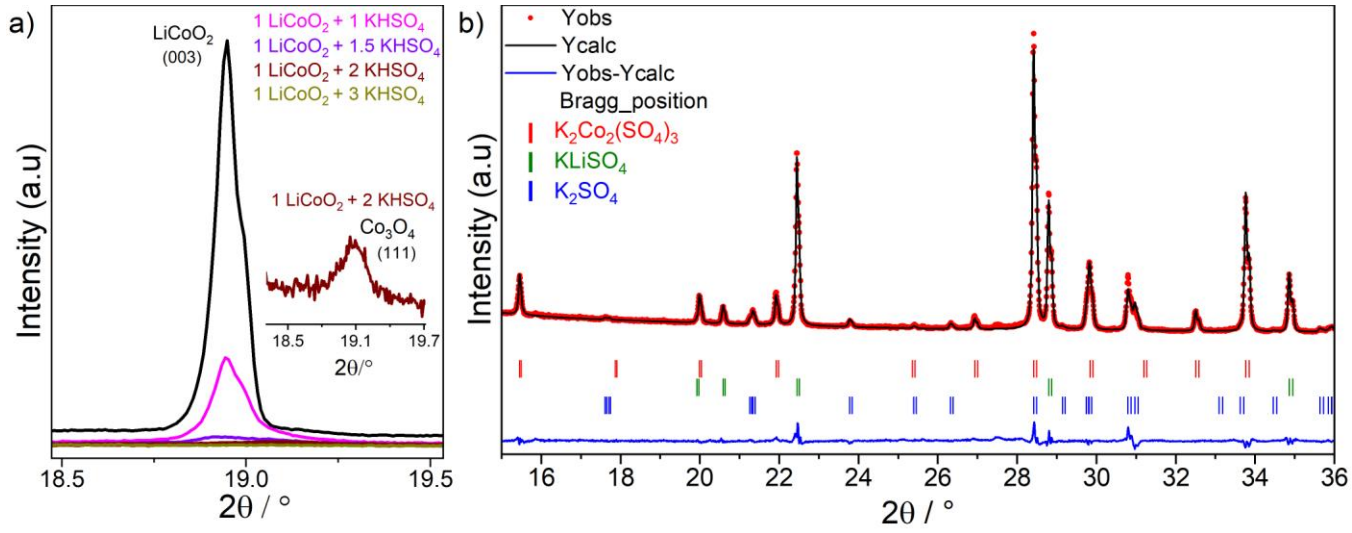

Figure 2. a) Evolution of the Bragg (003) reflection of $LiCoO_2$ as a function of the content of $KHSO_4$, denoted *n*. $KHSO_4$: [$LiCoO_2$: *n*$KHSO_4$]. b) Rietveld refinement of the XRD pattern of the sample [$LiCoO_2$: 3$KHSO_4$] after the heat treatment.

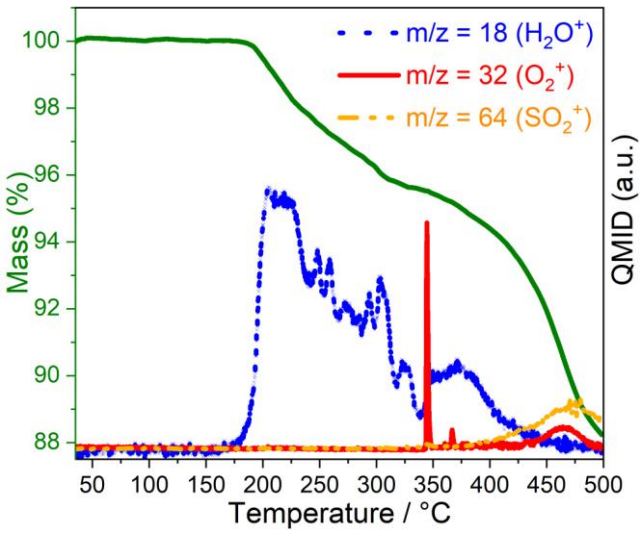

Figure 3. Thermogravimetric experiment coupled with mass spectrometry of [$LiCoO_2$: 3$KHSO_4$] obtained under argon atmosphere.

Structural evolution

The reaction of $LiCoO_2$ with $KHSO_4$ is particular as it involves the melting of the salt. To capture such a difference in reactivity, differential scanning calorimetry (DSC) was performed. The corresponding curve obtained under argon is shown in **Figure 4**. Upon heating, a first endothermic peak is detected at 183°C and was assigned to a phase transition[37] of $KHSO_4$ **(Figure S2)**. Then, an intense peak is detected at 203°C which corresponds to the melting of $KHSO_4$[37–39] highlighting the change in the reactivity from a solid-solid to a solid-liquid reaction. Then, one exothermic peak characteristic of a phase crystallization is detected at 212°C and a broad diffuse exothermic peak is finally observed at 302 °C.

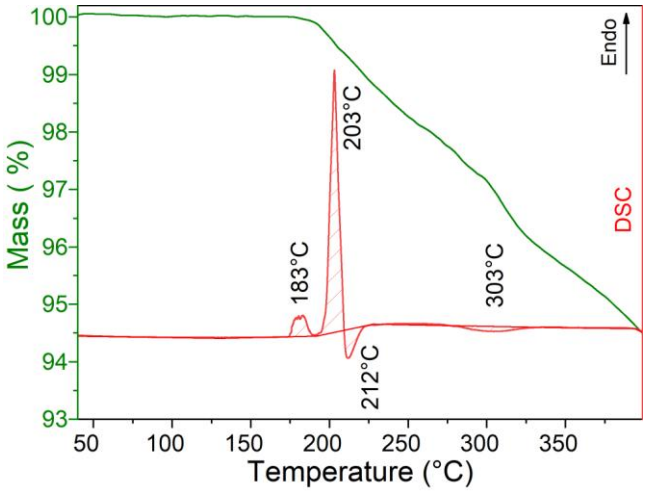

Figure 4. Thermal analyses TGA and DSC curves of [$LiCoO_2$: 3$KHSO_4$] mixture.

The structural phase evolution was first investigated using variable-temperature XRD analysis. Beyond 200 °C, the melting of $KHSO_4$ leads to the loss of XRD signal with diffuse scattering preventing further analysis. The evolution of XRD patterns collected from RT to 200 °C is displayed in **Figure 5**. From 30°C to 180°C, the Bragg peaks of the precursors slightly shift to lower angles, consistent with the unit cell thermal

expansion. At 175°C, new peaks appear that can be assigned to a phase transition of $KHSO_4$ of higher symmetry[40] featuring a high proton conductivity, *i.e.*, 10^{-1} S/cm[41]. This phase transition corresponds to the endothermic peak detected around 183 °C on the DSC curve. At 180 °C, a phase indexed to $K_4LiH_3(SO_4)_4$ (tetragonal, S.G: $P4_1$)[42] appears indicating a delithiation of $LiCoO_2$ and the departure of protons from $KHSO_4$. Considering a charge compensating mechanism, we hypothesized an ionic exchange between the two phases. In addition, we observed a continuous shift to lower 2θ values of $LiCoO_2$ (003) Bragg reflection upon heating, which can originate from either/both the thermal cell expansion and the removal of layered Li^+ ions inducing an increase of the *c*-parameter, *i.e.*, a decrease of the (003) 2θ value, due to the repulsive electrostatic interaction between facing oxide ions[43]. The evolution of the *c*-parameter as a function of temperature, determined by profile matching, was monitored with and without the presence of $KHSO_4$ (**Figure S3**). The result shows that the presence of $KHSO_4$ only induces a slight deviation (about 0.12 Å) from the expected linear increase of the *c*-parameter due to crystal structure thermal expansion. The observation of $K_4LiH_3(SO_4)_4$ suggests that proton could be inserted within the structure, possibly impacting the stacking of slabs and in turn the *c*-parameter. Such a Li^+/H^+ ion exchange will be examined later.

To follow the phase evolution beyond the melting temperature of $KHSO_4$, we used *ex situ* x-ray diffraction on samples treated at 200 and 300 °C **(Figure S4)**. The XRD patterns obtained at both temperatures reveal the presence of a reduced hydroxysulfate phase composition, $Co_3(SO_4)_2(OH)_2$. We assigned the appearance of this phase to the first exothermic peak detected at 212 °C on the DSC curve **(figure 3)**. This phase thus crystallizes just after the melting of the salt and is an intermediate prior to the formation of the langbeinite compound $K_2Co_2(SO_4)_3$.

To probe the oxidation state and the local structure of cobalt during the reaction of $LiCoO_2$ with $KHSO_4$, we used a homemade cell[27] allowing a temperature-controlled *in situ* X-ray absorption spectroscopy (XAS) at the Co K-edge, *i.e.*, 7709 eV. We first examined the XANES **(Figure 6a**) spectra recorded within the 180-200 °C temperature range where we observed H^+/Li^+ ionic exchange. In this range, a slight modification of the edge structure can be noticed at 200 °C. The refinements of the Co K-edge extended fine structure (EXAFS) spectrum indicate the occurrence of regular CoO_6 octahedra (6×1.91 Å) at the early stage of H^+/Li^+ ionic exchange, *i.e.*, at 180 °C. At 200 °C, however, the best fit was obtained by the occurrence of a distortion of the CoO_6 octahedra with long Co-O bond distances **(Figure 6b, Table 1)**. Such a bond increase can be assigned to the formation of O-H bonds consistent with the hypothesized Li^+/H^+ ionic exchange between $LiCoO_2$ and $KHSO_4$. Beyond the melting temperature, we observed a continuous shift of the absorption edge to lower energy **(Figure 6c**) consistent with the formation of reduced compounds $Co_3(SO_4)_2(OH)_2$ and $K_2Co_2(SO_4)_3$. After cooling back to room temperature, the measured XANES spectrum was fitted using a linear combination consisting of $K_2Co_2(SO_4)_3$, which confirms the completion of the reaction **(Figure 6d, Table S2)**. Note that a small impurity of Co_3O_4, was detected **(Figure S5)**.

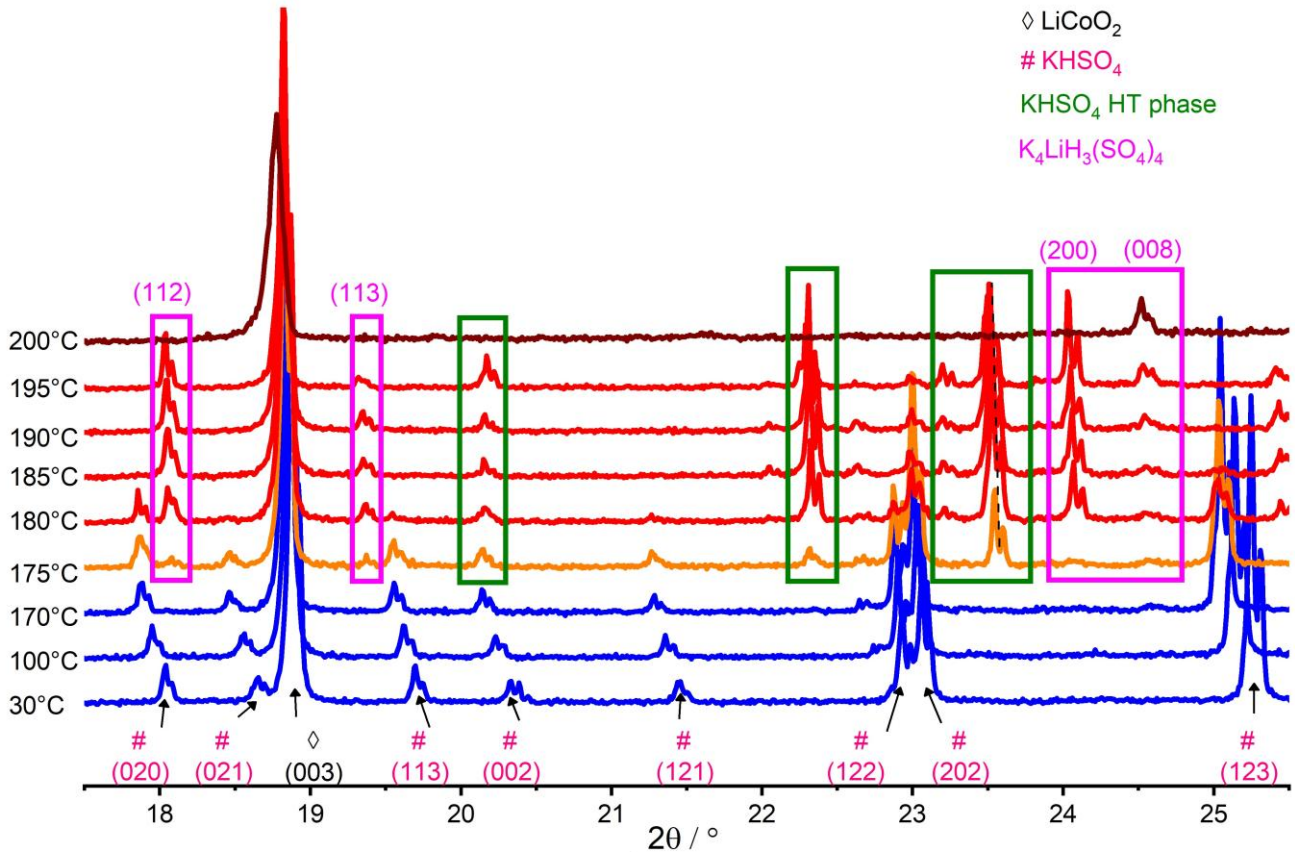

Figure 5. Variable-temperature x-ray diffraction analysis performed on a mixture [$LiCoO_2$: $3KHSO_4$].

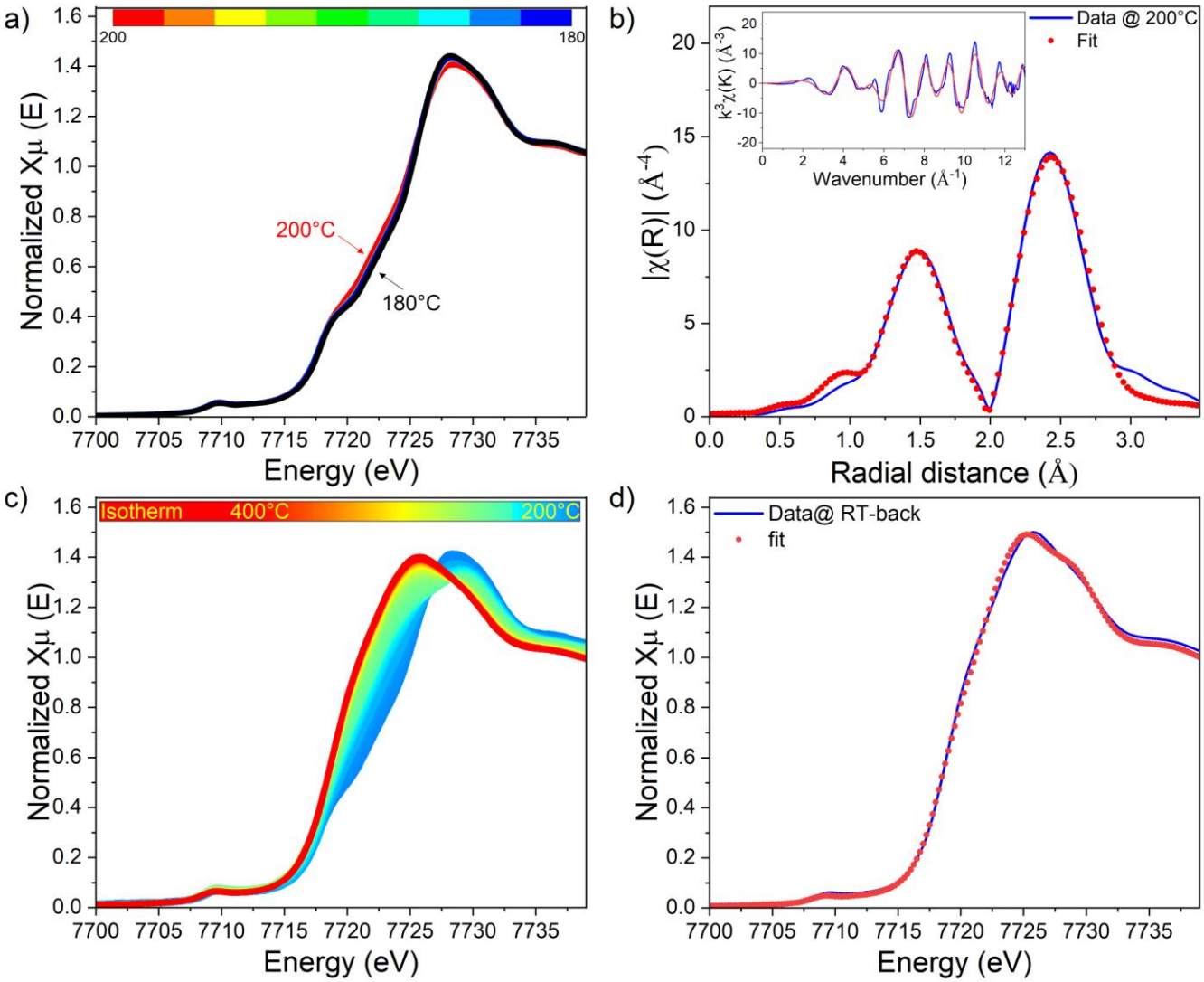

Figure 6. Variable-temperature X-ray Absorption Spectroscopy data during a thermal treatment of pristine $LiCoO_2$ with $KHSO_4$ [1:3] (a) within the 180-200 °C and (b) 200-400 °C temperature ranges. C) Fourier transformation of Co K-edge EXAFS of pristine [$LiCoO_2$: 3 $KHSO_4$] at 200°C and it fit. d) linear combination fitting of XANES spectrum of [$LiCoO_2$: $3KHSO_4$] at RT-back.

Table 1. Parameters obtained from the refinements of the EXAFS spectrum of $LiCoO_2$: $KHSO_4$ [1:3] collected at 200°C considering two models, with and without Co ion distortion.

Models	**R-factor**	**Atoms**	**N**	**E_0 (eV)**	**Amp**	**σ^2**	**R (Å)**	**R reference (Å)**
un-distorted	0.042	Co-O	6	-5.897	0.61	0.00480 (±0.0009)	1.918 (±0.006)	1.921
		Co-Co	6	-5.897	0.61	0.00285 (±0.0005)	2.813 (±0.0044)	2.816
distorted	0.008	Co-O	5.3	-5.308	0.61	0.0029 (±0.002)	1.906 (±0.013)	1.921
		Co-O2	0.7	-5.308	0.61	0.0028 (±0.018)	2.367 (±0.122)	1.921
		Co-Co	6	-5.308	0.61	0.0032 (±0.0007)	2.825 (±0.010)	2.816

The Li^+/H^+ exchange reaction between the two reactants is the first step toward the salt conversion of the layered structure with a complex mechanism. As no analogue system can be found in the literature, we further investigate it using DFT-calculations. First, it can be hypothesized that the mechanism involved is likely activated by the protonation of the highly reactive oxygen-terminated surface of $LiCoO_2$ and the Li^+ diffusion towards the H-defective $KHSO_4$ phase for charge compensation. The delithiation of $LiCoO_2$ is known to cause the destabilization of oxide ions that can recombine to release molecular oxygen (oxidative condition). However, our thermal analysis data show that the departure of O_2 occurs at a temperature higher than delithiation, hence supporting the Li^+/H^+ exchange as a charge compensating mechanism. To better understand such Li^+/H^+ exchange reaction, we performed DFT-calculations seeking to compare the energy between two models: a Li-defective one and a Li/H-substituted one. In addition, we considered two sets of configurations where defects and protons are either far or close to each other. **Figure 7a** displays the evolution for both configurations of the relative difference in energy between the Li/H-substituted and Li-defective models as a function of composition. It reveals that whatever the configuration, the $Li_{1-x}H_xCoO_2$ solid solution is thermodynamically favored over the sole delithiation of $LiCoO_2$. Within the probed compositional range of $Li_{1-x}H_xCoO_2$, we observed that the structure is not particularly altered by the Li^+/H^+ substitution. As expected by the inductive effect[44] of proton, we observed the formation of O-H covalent bonds associated with a slight increase of the Co-OH bonds, consistent with XAS data. Interestingly, for a Li^+/H^+ substitution equals to x=1/4 having close H atoms in the alkali layer, we found a spontaneous formation of H_2O molecules **(Figure 7b)** after full structural relaxation leading to a thermodynamically stable product (200meV per formula unit lower in energy than the non- dehydrated structures as indicated by the arrow on **(Figure 7a)**. Such spontaneous dehydration requires high statistical occurrence of local H···H configurations, which is favored at the interface scale. It is therefore likely that, in addition to promoting Li^+/H^+ exchange at the $LiCoO_2/KHSO_4$ interfaces, temperature also facilitates the migration of H^+ to generate these H···H configurations and release H_2O. The dehydration process leads to the destabilization/reduction of the Co ions, *i.e.*, nearest cobalt ions become five-fold coordinated **(Figure 7c)**. This may ultimately trigger the attack of HSO_4^-/SO_4^{2-} anions occurring in the melt at 210 °C, as shown by the formation of the hydroxy-sulfate phase $Co_3(SO_4)_2(OH)_2$ in our *ex situ* XRD experiments.

To sum up, the reaction mechanism of $LiCoO_2$ with $KHSO_4$ first involves Li ions and proton exchange between the layered structure and $KHSO_4$. It has been suggested that the reaction takes place at the interface between the reactive oxygen-terminated surface of $LiCoO_2$ driving the Li^+ diffusion towards the H-defective $KHSO_4$ phase for charge compensation. The thermal activation yields a proton and Li diffusion toward the bulk, as shown by the formation of $K_4LiH_3(SO_4)_4$ revealed by XRD data. The greater phase stability of $Li_{1-x}H_xCoO_2$ compared to the delithiated phase, as deduced from DFT-calculations, is consistent with the Li^+/H^+ exchange and the onset of spontaneous dehydration of the layered structure (observed even at 0K in our calculations), agrees with the progressive dehydration observed by thermal analysis. Such a dehydration leads to under-coordinated Co ions that can act as reactive sites for sulfation, likely involving melted HSO_4^- ionic species, as revealed by the formation of the reduced intermediate phase $Co_3(SO_4)_2(OH)_2$. The later phase is then transformed toward the langbeinite $K_2Co_2(SO_4)_3$ phase involving dehydration and potassium intercalation. Overall, this analysis shed new light into the complex mechanism underlying the salt conversion of $LiCoO_2$.

Extension to NMC and NCA cathode materials

The continuous technological development in LIB has led to the development of positive electrodes with novel chemical composition spanning over LCO, NMC, NCA, and eventually to Co-free composition. Such a variety of chemistry adds complexity to the recycling processes and should be taken into account when exploring alternative routes[45]. We then further extended the salt conversion route to these various material by concentrating on the case of NMC and NCA. **Figures 8a and 8b** display the Rietveld

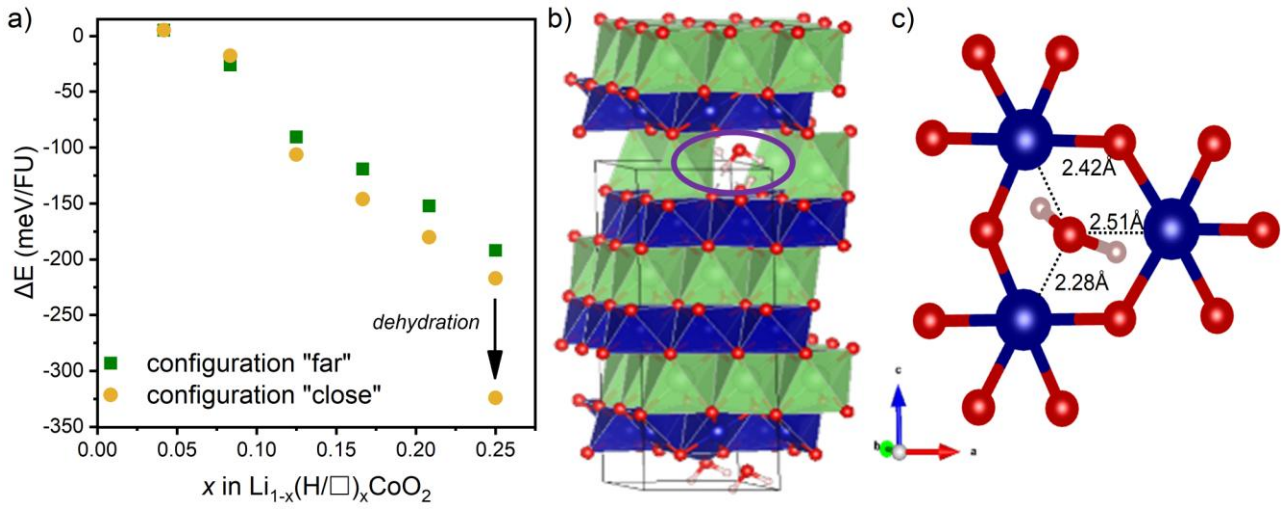

Figure 7. a) Relative energy (in meV per formula unit) of Li-defective $Li_{1-x}CoO_2$ and Li/H-substituted $LiCoO_2$ showing that the latter is thermodynamically favored over the former (see computational details). The arrow corresponds to the spontaneously structure with free

H_2O shown in b). b) Relaxed structure for a multilayer $Li_{1-x}H_xCoO_2$ with x=1/4. c) Example of the Co local environment obtained after full relaxation due to the Li^+/H^+ exchange, $Co\cdots OH_2$ distances are indicated to illustrate the formation of water molecule.

refinements of the XRD patterns of NMC and NCA treated with $KHSO_4$. For both NMC and NCA compositions, the XRD pattern was indexed with a single phase of cubic $K_2M_2(SO_4)_3$ structure suggesting the concomitant stabilization of Ni, Co and Mn within the cationic sublattice. To confirm the presence of the different cations in the 4a site of the langbeinite type structure, we plotted the unit cell parameters deduced from the Rietveld analysis as a function of the ionic radius **(Figure 8c)**. For NMC, the cubic unit cell parameter value 9.9593 Å lies within $K_2Ni_2(SO_4)_3$ and $K_2Mn_2(SO_4)_3$ confirming the stabilization of Ni, Co and Mn within the cubic structure with an estimated composition $K_2(Ni_{1/3}Co_{1/3}Mn_{1/3})_2(SO_4)_3$, which was further confirmed by x-ray energy dispersive spectroscopy **(Figure 8d)**. For NCA, the unit cell parameter is closer to that of $K_2Ni_2(SO_4)_3$ also suggesting the stabilization of Ni and Co within the cubic structure. Moreover, small peaks (*) located at 12.25°; 27.53°; 32.65°; 41.29° and 58.71 ° were identified as $K_3Al(SO_4)_3$ (structure unsolved), showing that Al^{3+} ions are also stabilized in a sulfate-based network. Based on the above results, equations (3) and (4) were proposed for NMC and NCA, which were further confirmed by quantitative-phase analyses obtained by Rietveld refinements **(Table S3)**

$$1Li(Ni_{1/3}Co_{1/3}Mn_{1/3})O_2 + 3KHSO_4 \rightarrow \frac{1}{2}K_2(Ni_{1/3}Co_{1/3}Mn_{1/3})_2(SO_4)_3 + KLiSO_4 + \frac{1}{2}K_2SO_4 + \frac{1}{4}O_{2(g)} + \frac{3}{2}H_2O_{(g)} \quad \text{(eq.3)}$$

$$1Li(Ni_{0.82}Co_{0.15}Al_{0.03})O_2 + 3\,KHSO_4 \rightarrow 0.48K_2(Ni_{0.85}Co_{0.15})_2(SO_4)_3 + KLiSO_4 + 0.47\,K_2SO_4 + 0.03K_3Al(SO_4)_3 + \frac{1}{4}O_{2(g)} + \frac{3}{2}H_2O_{(g)} \quad \text{(eq. 4)}$$

All in all, these results confirm the transferability of this approach to the wide family of transition metal oxides which provide experimentalist with economic and environmentally friendly procedure to recycle their post-mortem batteries.

Metals recovery

To illustrate the possibility to recover metals using the salt conversion, we highlight $LiCoO_2$ as an example. We first prepared an aqueous solution by dissolving the sulfate-based products (see experimental section). The recovery of Co and Li ions was performed by a selective precipitation and the corresponding XRD patterns of the products are gathered in **Figure 9**. Cobalt ions were precipitated as an oxalate salt $CoC_2O_4(H_2O)_2$ using $K_2C_2O_4$. The yield of the reaction determined by complexometry of the filtrate was 91%. Prior to the recovery of lithium, sulfates were removed

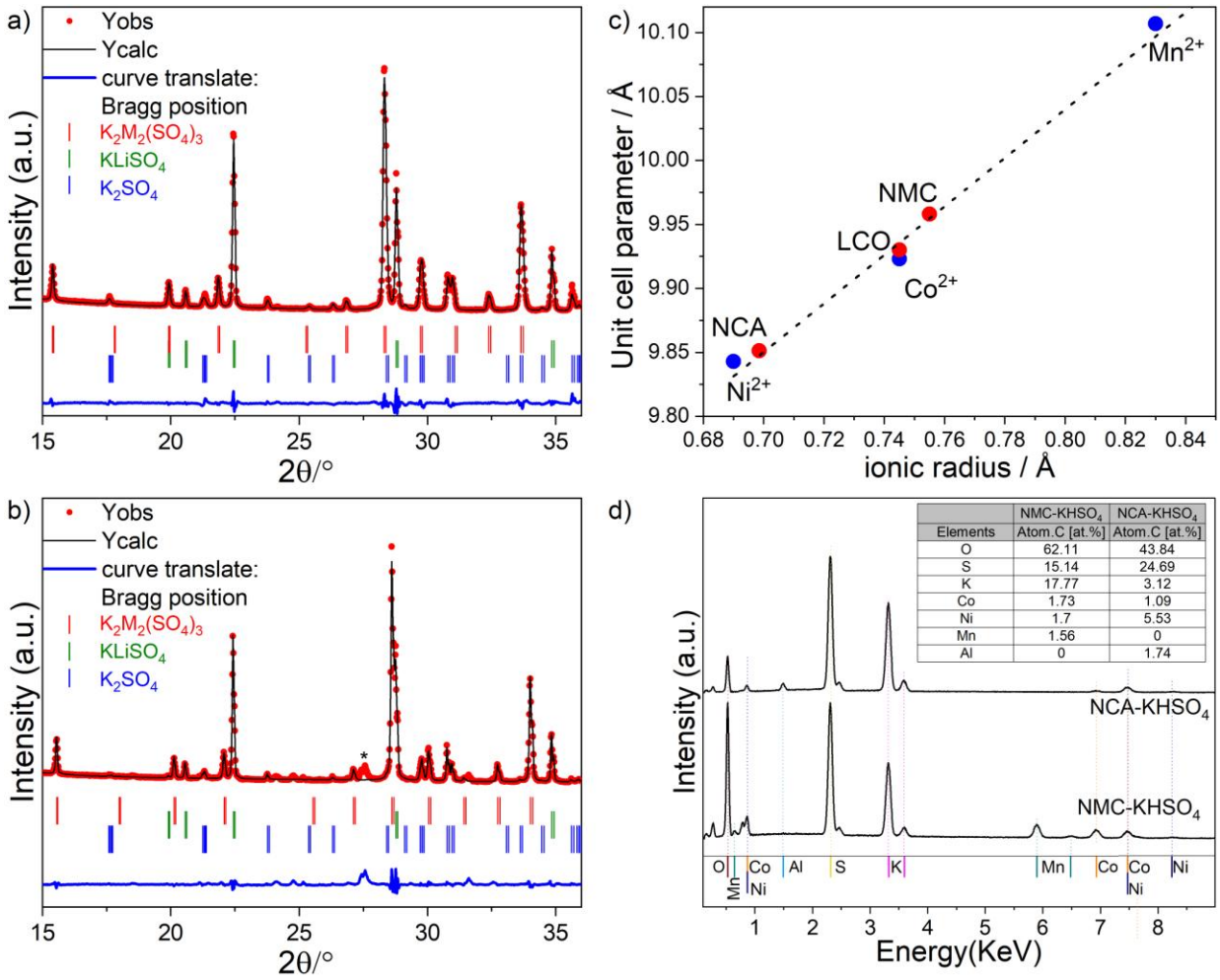

Elements	NMC-$KHSO_4$ Atom.C [at.%]	NCA-$KHSO_4$ Atom.C [at.%]
O	62.11	43.84
S	15.14	24.69
K	17.77	3.12
Co	1.73	1.09
Ni	1.7	5.53
Mn	1.56	0
Al	0	1.74

Figure 8. Rietveld refinements of XRD patterns of a) NMC and b) NCA after heat treatment with $KHSO_4$. c) Unit cell parameters of $K_2Ni_2(SO_4)_3$, $K_2Co_2(SO_4)_3$, $K_2Mn_2(SO_4)_3$ and LCO, NMC, and NCA heat-treated with $KHSO_4$, versus ionic radius of M with M= (Ni^{2+}, Co^{2+}, Mn^{2+}). d) X-ray energy dispersive spectroscopy of NCA and NMC treated with $KHSO_4$ and heated at 400°C for 4h under air.

by addition of barium chloride, resulting in the immediate precipitation of $BaSO_4$. Finally, lithium was precipitated as a Li_3PO_4 phosphate phase with a gravimetric yield of 78 %. Overall, this shows that sulfate-based aqueous solution is suited to recover the targeted elements.

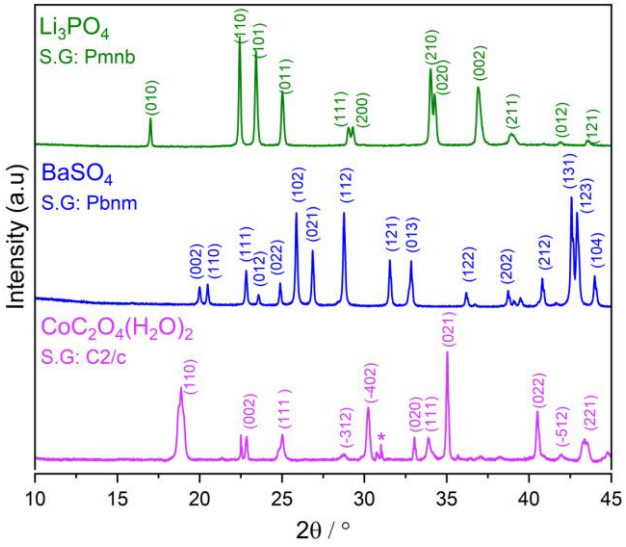

Figure 9. XRD patterns collected at different stages of metals recovery: precipitation of Co-oxalate hydrate, neutralization of

sulfates anions: precipitation of $BaSO_4$ and precipitation of Li_3PO_4. S.G refers to space group.

CONCLUSION

We have here explored the reactivity of lithiated transition metal oxide with potassium hydrogenosulfate. Our motivation was based on the occurrence of a defined compound $K_2M_2(SO_4)_3$ that features a large compositional versatility including cobalt, nickel and manganese cations. Based on a salt conversion approach, we seek the conditions adapted for converting the layered transition metal oxides into sulfate-based products to enable subsequent metals recovery using only water as a medium, which therefore prevents the classical use of highly acidic solutions usually used in hydrometallurgy to destabilize the oxidic compounds. Both the temperature and the salt content were shown to be decisive parameters to complete the oxide to sulfate transformation. Most interestingly, we were able to decipher the reaction mechanism in the case of $LiCoO_2$. Using variable-temperature XRD and XAS analyses, we rationalized the complete reaction pathway that first involves surface-activated Li^+ ions and proton exchange between $LiCoO_2$ and $KHSO_4$ reactants. At mild temperature, $KHSO_4$ first undergoes a high-symmetry phase transition featuring high proton conductivity. Subsequently, Li^+/H^+ exchange is evidenced by the formation of $K_4LiH_3(SO_4)_4$, suggests the concomitant formation of $Li_{1-x}H_xCoO_2$. X-ray absorption spectroscopy showed that Li^+/H^+ exchange leads to the distortion of CoO_6 octahedra which was assigned to the formation of longer Co-OH bonds compared to Co-O bonds. DFT-calculations revealed that the accumulation of proton can eventually yield a spontaneous dehydration which is thought to be favoured by thermal activation, therefore yielding under-coordinated Co ions prone to react with melted HSO_4^-/SO_4^{2-} species, as shown by the crystallization of $Co_3(SO_4)_2(OH)_2$. Finally, the latter is then transformed toward the langbeinite $K_2Co_2(SO_4)_3$ phase involving dehydration and potassium intercalation. The extension of the salt conversion to NMC and NCA compounds supports the versatility of this method for different types of electrode chemistry of LIB, opening practical outcomes to the vital question of battery recycling.

ASSOCIATED CONTENT

Supporting Information. Rietveld analyses; thermal analyses and thermo-diffraction of $KHSO_4$; Unit cell parameters of $LiCoO_2$ upon thermal treatment with and without $KHSO_4$; XRD analysis of treated samples at 200 and 300 °C; XRD analysis of the recovered sample after in situ XAS analysis.

AUTHOR INFORMATION

Corresponding Author

*To whom correspondence should be addressed.

damien.dambournet@sorbonne-universite.fr

Notes

The authors declare no competing financial interest.

ACKNOWLEDGMENTS

XAS measurements were performed at the beamline ROCK of synchrotron Soleil (Gif-sur-Yvette, France). Synchrotron Soleil (France) is acknowledged for providing beamtime at the beamline ROCK. This work was supported by two public grants overseen by the French National Research Agency (ANR) as part of the "Investissements d'Avenir" program (Projects ANR-10-EQPX-45, Equipex ROCK) and ANR-RELIABLE (ANR-18-CE05-0031). We thank Matthieu Courty for conducting thermal analyses and Tifany Phou for preliminary experiments.

REFERENCES

(1) Hodgkinson, J. H.; Smith, M. H. Climate Change and Sustainability as Drivers for the next Mining and Metals Boom: The Need for Climate-Smart Mining and Recycling. *Resources Policy* **2018**, 101205.

(2) Pillot, C. Lithium Ion Battery Raw Material Supply & Demand 2016-2025. http://cii-resource.com/cet/AABE-03-17/Presentations/BRMT/Pillot_Christophe.pdf (accessed 2024-02-01)

(3) Greim, P.; Solomon, A. A.; Breyer, C. Assessment of Lithium Criticality in the Global Energy Transition and Addressing Policy Gaps in Transportation. *Nat Commun* **2020**, *11* (1), 4570.

(4) Nie, H.; Xu, L.; Song, D.; Song, J.; Shi, X.; Wang, X.; Zhang, L.; Yuan, Z. LiCoO2: Recycling from Spent Batteries and Regeneration with Solid State Synthesis. *Green Chem.* **2015**, *17* (2), 1276–1280.

(5) Shi, Y.; Zhang, M.; Meng, Y. S.; Chen, Z. Ambient-Pressure Relithiation of Degraded $Li_xNi_{0.5}Co_{0.2}Mn_{0.3}O_2$ ($0 < x < 1$) via Eutectic Solutions for Direct Regeneration of Lithium-Ion Battery Cathodes. *Advanced Energy Materials* **2019**, *9* (20), 1900454.

(6) Wang, T.; Luo, H.; Bai, Y.; Li, J.; Belharouak, I.; Dai, S. Direct Recycling of Spent NCM Cathodes through Ionothermal Lithiation. *Advanced Energy Materials* **2020**, *10* (30), 2001204.

(7) Chagnes, A.; Pospiech, B. A Brief Review on Hydrometallurgical Technologies for Recycling Spent Lithium-Ion Batteries. *J. Chem. Technol. Biotechnol.* **2013**, *88* (7), 1191–1199.

(8) Tran, M. K.; Rodrigues, M.-T. F.; Kato, K.; Babu, G.; Ajayan, P. M. Deep Eutectic Solvents for Cathode Recycling of Li-Ion Batteries. *Nature Energy* **2019**, *4* (4), 339.

(9) Zhang, X.; Li, L.; Fan, E.; Xue, Q.; Bian, Y.; Wu, F.; Chen, R. Toward Sustainable and Systematic Recycling of Spent Rechargeable Batteries. *Chem. Soc. Rev.* **2018**, *47* (19), 7239–7302.

(10) Mao, J.; Ye, C.; Zhang, S.; Xie, F.; Zeng, R.; Davey, K.; Guo, Z.; Qiao, S. Toward Practical Lithium-Ion Battery Recycling: Adding Value, Tackling Circularity and Recycling-Oriented Design. *Energy Environ. Sci.* **2022**, *15* (7), 2732–2752.

(11) Wang, D.; Wen, H.; Chen, H.; Yang, Y.; Liang, H. Chemical Evolution of $LiCoO_2$ and $NaHSO_4 \cdot H_2O$ Mixtures with Different Mixing Ratios during Roasting Process. *Chem. Res. Chin. Univ.* **2016**, *32* (4), 674–677.

(12) Wang, D.; Zhang, X.; Chen, H.; Sun, J. Separation of Li and Co from the Active Mass of Spent Li-Ion Batteries by Selective Sulfating Roasting with Sodium Bisulfate and Water Leaching. *Minerals Engineering* **2018**, *126*, 28–35.

(13) Chen, X.; Luo, C.; Zhang, J.; Kong, J.; Zhou, T. Sustainable Recovery of Metals from Spent Lithium-Ion Batteries: A Green Process. *ACS Sustainable Chem. Eng.* **2015**, *3* (12), 3104–3113.

(14) Tang, Y.; Qu, X.; Zhang, B.; Zhao, Y.; Xie, H.; Zhao, J.; Ning, Z.; Xing, P.; Yin, H. Recycling of Spent Lithium Nickel Cobalt Manganese Oxides via a Low-Temperature Ammonium Sulfation Roasting Approach. *Journal of Cleaner Production* **2021**, *279*, 123633.

(15) *Lide, D. R. CRC Handbook of Chemistry and Physics: [A Ready-Reference Book of Chemical and Physical Data], 88th ed. (2007-2008).; CRC : Taylor & Francis: Boca Raton, Fla., London, 2008.*

(16) Dutta, A.; Swain, D.; Sunil, J.; Narayana, C.; Guru Row, T. N. Minerals to Functional Materials: Characterization of Structural Phase Transitions and Raman Analysis of a Superionic Phase in $Na_6Co(SO_4)_4$. *Inorg. Chem.* **2020**, *59* (12), 8424–8431.

(17) Dwibedi, D.; Gond, R.; Dayamani, A.; Araujo, R. B.; Chakraborty, S.; Ahuja, R.; Barpanda, P. $Na_{2.32}Co_{1.84}(SO_4)_3$ as a New Member of the Alluaudite Family of High-Voltage Sodium Battery Cathodes. *Dalton Trans.* **2016**, *46* (1), 55–63.

(18) Fry, A. M.; Sweeney, O. T.; Adam Phelan, W.; Drichko, N.; Siegler, M. A.; McQueen, T. M. Unique Edge-Sharing Sulfate-Transition Metal Coordination in $Na_2M(SO_4)_2$ (M=Ni and Co). *Journal of Solid State Chemistry* **2015**, *222*, 129–135.

(19) Speer, D.; Salje, E. Phase Transitions in Langbeinites I: Crystal Chemistry and Structures of K-Double Sulfates of the Langbeinite Type M2++$K_2(SO_4)_3$, M++=Mg, Ni, Co, Zn, Ca. *Phys Chem Minerals* **1986**, *13* (1), 17–24.

(20) Zemann, A.; Zemann, J. Die Kristallstruktur von Langbeinit, $K_2Mg_2(SO_4)_3$. *Acta Cryst* **1957**, *10* (6), 409–413.

(21) Oelkrug, H.; Brückel, T.; Hohlwein, D.; Hoser, A.; Prandl, W. The Magnetic Structure of the Langbeinite $K_2Mn_2(SO_4)_3$. *Phys Chem Minerals* **1988**, *16* (3), 246–249.

(22) Lander, L.; Rousse, G.; Batuk, D.; Colin, C. V.; Dalla Corte, D. A.; Tarascon, J.-M. Synthesis, Structure, and Electrochemical Properties of K-Based Sulfates $K_2M_2(SO_4)_3$ with M = Fe and Cu. *Inorg. Chem.* **2017**, *56* (4), 2013–2021.

(23) Moriyoshi, C.; Itoh, K.; Hikita, T. Structural Study of Phase Transition in $K_2Co_2(SO_4)_3$ Crystals. *J. Phys. Soc. Jpn.* **1995**, *64* (12), 4726–4732.

(24) Moriyoshi, C.; Itoh, K. Structural Study of Phase Transition Mechanism of Langbeinite-Type $K_2Zn_2(SO_4)_3$ Crystals. *J. Phys. Soc. Jpn.* **1996**, *65* (11), 3537–3543.

(25) Percival, M. J. L.; Schmahl, W. W.; Salje, E. Structure of Cobalt Doped $K_2Cd_2(SO_4)_3$ Langbeinite at Three Temperatures above the P213-P212121 Phase Transition, and a New Trigger Mechanism for the Ferroelastic Transformation. *Phys Chem Minerals* **1989**, *16* (6), 569–575.

(26) Rodríguez-Carvajal, J. Recent Advances in Magnetic Structure Determination by Neutron Powder Diffraction. *Physica B: Condensed Matter* **1993**, *192* (1), 55–69.

(27) Safarzadeh, Z.; Gomes, J. C.; Sirieix-Plénet, J.; Ruiz, N.; Hamitouche, L.; Michot, L.; Carré, L.; Barthe, L.; Briois, V.; Rollet, A.-L. Advanced Design of a X-Ray Absorption Spectroscopy Setup for Measuring Transition Metals Speciation in Molten Carbonates, Hydroxides and Hydrogenosulfates. *Review of Scientific Instruments* **2022**, *93* (7), 075102..

(28) Kresse, G.; Furthmüller, J. Efficiency of Ab-Initio Total Energy Calculations for Metals and Semiconductors Using a Plane-Wave Basis Set. *Computational Materials Science* **1996**, *6* (1), 15–50.

(29) Kresse, G.; Joubert, D. From Ultrasoft Pseudopotentials to the Projector Augmented-Wave Method. *Phys. Rev. B* **1999**, *59* (3), 1758–1775.

(30) Blöchl, P. E. Projector Augmented-Wave Method. *Phys. Rev. B* **1994**, *50* (24), 17953–17979.

(31) Perdew, J. P.; Burke, K.; Ernzerhof, M. Generalized Gradient Approximation Made Simple. *Phys. Rev. Lett.* **1996**, *77* (18), 3865–3868.

(32) Dudarev, S. L.; Botton, G. A.; Savrasov, S. Y.; Humphreys, C. J.; Sutton, A. P. Electron-Energy-Loss Spectra and the Structural Stability of Nickel Oxide: An LSDA+U Study. *Phys. Rev. B* **1998**, *57* (3), 1505–1509.

(33) Harris, W. F.; Sweet, T. R. Volumetric Determination of Cobalt. *Anal. Chem.* **1954**, *26* (10), 1649–1651.

(34) Moriyoshi, C.; Itoh, K.; Hikita, T. Structural Study of Phase Transition in $K_2Co_2(SO_4)_3$ Crystals. *J. Phys. Soc. Jpn.* **1995**, *64* (12), 4726–4732.

(35) Bhakay-Tamhane, S.; Sequiera, A.; Chidambaram, R. Structure of Lithium Potassium Sulphate, $LiKSO_4$: A Neutron Diffraction Study. *Acta Cryst C* **1984**, *40* (10), 1648–1651.

(36) McGinnety, J. A. Redetermination of the Structures of Potassium Sulphate and Potassium Chromate: The Effect of Electrostatic Crystal Forces upon Observed Bond Lengths. *Acta Cryst B* **1972**, *28* (9), 2845–2852.

(37) Tahoov, K. K.; ABOSEHLY, A. M.; EL-SHARKAWY, A. A. THERMAL STUDY OF THE PHASE TRANSITIONS IN POTASSIUM HYDROGEN SULFATE $KHSO_4$. *Acta Physica Polonica A* **1984**, 86(3), 349-355.

(38) Vries, K. J. de; Gellings, P. J. The Thermal Decomposition of Potassium and Sodium-Pyrosulfate. *POLYHEDRON* **1969**, *31* (5), 1307–1313.

(39) Diosa, J. E.; Vargas, R. A.; Mina, E.; Torijano, E.; Mellander, B.-E. Phase Transitions of KHSO4 above Room Temperature. *physica status solidi (b)* **2000**, *220* (1), 641–645.

(40) Swain, D.; Bhadram, V. S.; Pradhan, G. K.; Bhat, S. V.; Narayana, C.; Rao, C. N. R. Superionic Phase Transition in KHSO4: A Temperature-Dependent Raman Investigation. *J. Phys. Chem. A* **2010**, *114* (37), 10040–10044.

(41) YOSHIDA, Y.; MATSUO, Y.; IKEHATA, S. NMR Study on Phase Transitions in $KHSO_4$. *Ferroelectrics* **2004**, *302* (1), 85–90.

(42) Nalini, G.; Row, T. N. G. Phase Transitions in $A_4Li(HSO_4)_3(SO_4)$; A = Rb, K: Single Crystal X-Ray Diffraction Studies. *J Chem Sci* **2003**, *115* (5), 473–490.

(43) Mizushima, K.; Jones, P. C.; Wiseman, P. J.; Goodenough, J. B. Li_xCoO_2. *Materials Research Bulletin* **1980**, *15* (6), 783–789.

(44) Padhi, A. K.; Nanjundaswamy, K. S.; Masquelier, C.; Okada, S.; Goodenough, J. B. Effect of Structure on the Fe^{3+}/Fe^{2+} Redox Couple in Iron Phosphates. *J. Electrochem. Soc.* **1997**, *144* (5), 1609.

(45) Bai, Y.; Muralidharan, N.; Sun, Y.-K.; Passerini, S.; Stanley Whittingham, M.; Belharouak, I. Energy and Environmental Aspects in Recycling Lithium-Ion Batteries: Concept of Battery Identity Global Passport. *Materials Today* **2020**, *41*, 304–315.

TOC

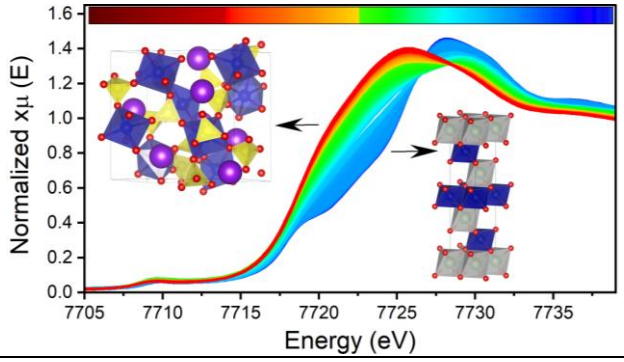
Normalized xμ (E)
1.6
1.4
1.2
1.0
0.8
0.6
0.4
0.2
0.0
7705
7710
7715
7720
7725
7730
7735
Energy (eV)